^{1}H CSA Parameters by Ultrafast MAS NMR: Measurement and Applications to Structure Refinement

Habeeba K. Miah†, Rosalie Cresswell†, Dinu Iuga‡ and Jeremy J. Titman†*

†*School of Chemistry, University of Nottingham, University Park, Nottingham, NG7 2RD, UK*

‡*UK 850 MHz Solid-state NMR Facility, Department of Physics, Millburn House, University of Warwick, Coventry, CV4 7AL, UK*

**Corresponding author: Email: Jeremy.Titman@nottingham.ac.uk, Tel: +44 115 951 3560*

Abstract

A ^{1}H anisotropic-isotropic chemical shift correlation experiment which employs symmetry-based recoupling sequences to reintroduce the chemical shift anisotropy in ν_1 and ultrafast MAS to resolve ^{1}H sites in ν_2 is described. This experiment is used to measure ^{1}H shift parameters for L-ascorbic acid, a compound with a relatively complex hydrogen-bonding network in the solid. The ^{1}H CSAs of hydrogen-bonded sites with resolved isotropic shifts can be extracted directly from the recoupled lineshapes. In combination with DFT calculations, hydrogen positions in crystal structures obtained from X-ray and neutron diffraction are refined by comparison with simulations of the full two-dimensional NMR spectrum. The improved resolution afforded by the second dimension allows even unresolved hydrogen-bonded sites ^{1}H to be assigned and their shift parameters to be obtained.

Introduction

Measurements of chemical shift parameters in solids for ^{1}H are challenging, because of the effects of strong homonuclear dipolar couplings and the relatively small chemical shift anisotropy (CSA). Nevertheless, several methods for measuring these parameters in solids have been demonstrated recently, based on two-dimensional magic angle spinning (MAS) experiments that correlate the anisotropic and isotropic parts of the shift interaction. These distinguish the different ^{1}H sites in the detection dimension and reintroduce or "recouple" the MAS-averaged ^{1}H CSA during the evolution time. For example, Brouwer and Ripmeester [1] resolved ^{1}H isotropic shifts in ν_2 by a combination of moderate MAS ($\omega_r/2\pi$ = 16 kHz) and multi-pulse homonuclear decoupling and used a recoupling sequence designed using symmetry principles [2,3] during

t_1. Subsequently, Hou *et al.* [4] optimized the resolution of ^{1}H sites by magnetization transfer to a neighbouring ^{15}N nucleus after recoupling the ^{1}H CSA in a similar fashion and measured the ^{1}H shift parameters for the amide sites in ^{15}N-enriched proteins. Miah *et al.* [5] employed modified recoupling sequences suitable for use with "ultrafast" MAS ($\omega_r/2\pi$ > 50 kHz), an approach that allows hydrogen-bonded sites in simple crystalline solids to be resolved in ν_2 without the need for multi-pulse homonuclear decoupling. Pandey *et al.* [6] improved this ultrafast MAS experiment by using composite pulses as the basis for similar CSA recoupling sequences, while Zhang *et al.* [7] used CSA recoupling as part of a three-dimensional DQ/CSA/SQ experiment which can be particularly useful when the resolution in the direct dimension is low.

It has been recognized for 30 years that solid-state ^{1}H NMR spectroscopy provides a way to study hydrogen bonding. For example, an early study [8] revealed a simple relationship between the ^{1}H isotropic chemical shift $\delta_{iso}(^1H)$ and the O…O distance in crystalline solids with moderate to strong hydrogen bonds. *Ab initio* calculations [9] suggested that the origin of this effect is the deshielding of the principal component of the ^{1}H shift tensor perpendicular to the hydrogen bond as the bond length decreases. Subsequently, a linear correlation between the isotropic ^{1}H shift $\delta_{iso}(^1H)$ and d(H…O) was established by comparison with neutron diffraction data [10]. Many similar relationships have been found for phosphates [11], hydrosilicates [12], selenites [13] and amino acids [14], and these are commonly used to extract hydrogen bond lengths from solid-state NMR measurements. However, later studies suggest that the situation is more complicated than first thought. The correlations are usually derived from a small set of samples with similar structure motifs and moderately strong hydrogen bonds, and scatter can be assigned to the sensitivity of the shift parameters to other aspects of the chemical environment of the ^{1}H nucleus, such as the nature of the donor and acceptor groups [15]. Furthermore, theoretical treatments in terms of bond polarization [16] or valence bond order [17] predict highly non-linear relationships between $\delta_{iso}(^1H)$ and d(H…O). More recently, Wu *et al.* [18] studied crystalline hydrates with relatively weak hydrogen bonds and found a clear correlation between both parallel and perpendicular components of the ^{1}H shift tensor and d(H…O). The parallel component becomes more shielded as the hydrogen bond length decreases, and as a result the span of the ^{1}H shift tensor provides a more sensitive indicator of hydrogen bond length than the isotropic average alone.

Recent work in this area involves the emerging field of "NMR crystallography" which combines measurements of solid-state NMR parameters with their calculation. For example, progress has been made

using high-resolution NMR correlation experiments to assign isotropic ^{1}H shifts [19] coupled with calculations using the gauge-including projector augmented-wave (GIPAW) approach [20]. X-ray diffraction is sensitive to electron density rather than to atomic positions, and so X-ray structures can be significantly improved using NMR crystallography. An early example [21] used DFT calculations of isotropic ^{1}H chemical shifts to refine the hydrogen positions for the hydrogen-bonded sites in polymorphs of methylnitroacetanilide, and the resulting hydrogen bond lengths were in close agreement with those measured by neutron diffraction. The ultimate goal of NMR crystallography is to develop "spectrum to structure" procedures [19] that involve identifying the actual crystal structure from an ensemble generated by structure prediction software without the need for diffraction methods. Recently the *de novo* structure determination of a pharmaceutical compound [22] has been demonstrated using a combination of solid-state ^{1}H NMR, crystal structure prediction methods [23] and DFT calculations.

In this contribution we show how the ultrafast MAS ^{1}H anisotropic-isotropic shift correlation experiment can be used to measure ^{1}H shift parameters for relatively complex hydrogen-bonded structures. As an example we present data for L-ascorbic acid which has eight distinct intermolecular hydrogen bonds, consisting of two helical series of OH…O bonds with the donor-acceptor sequence in each helix reversed for the two inequivalent molecules in the asymmetric unit. The ^{1}H CSAs of hydrogen-bonded ^{1}H sites with isotropic shifts which are resolved in ν_2 can be extracted directly from the recoupled lineshapes observed in ν_1. In addition, we demonstrate that hydrogen positions in crystal structures obtained from X-ray or neutron diffraction can be refined by a combination of DFT calculations and simulations of the full two-dimensional NMR spectrum. The improved resolution afforded by the second dimension allows even unresolved hydrogen-bonded sites ^{1}H to be assigned and their shift parameters to be obtained.

Pulse Sequence Design

Levitt and co-workers [2,3] applied symmetry principles to the design of recoupling sequences that reintroduce specific nuclear spin interactions averaged by MAS. This work makes use of the most flexible class of symmetry-based recoupling sequences, designated $\mathrm{R}N_n^\nu$, which consist of N composite inversion pulses R, timed to occupy n rotor periods τ_r. Each R element of the overall sequence has duration $n\tau_r/N$ and alternate elements have phases $\pm\pi\nu/N$. It has been shown [3] that the symmetry numbers N, n and ν

determine which interactions are retained in the first-order effective Hamiltonian for the sequence according to:

$$H^{(1)}_{lm\lambda\mu}(t_0) = \kappa_{lm\lambda\mu} A'_{lm} \exp\left\{ im\left(\alpha^0_{RL} - \omega_r t_0\right)\right\} T_{\lambda\mu} \quad \text{if}\left(nm - \nu\mu\right) = \frac{N}{2} k_\lambda$$

where A' is a rank-l irreducible spherical tensor operator describing the spatial part of the interaction Hamiltonian in the rotor frame, and T is a rank-λ irreducible spherical tensor operator describing the spin part in the laboratory frame. The rotational components of the spatial and spin tensors m and μ take values $m = l, l - 1, \ldots -l$ and $\mu = \lambda, \lambda - 1, \ldots -\lambda$, respectively, and k_λ is any integer with the same parity as λ. The scaling factor $\kappa_{lm\lambda\mu}$ describes the reduction in magnitude of the symmetry-allowed interaction that is an inevitable consequence of recoupling, and the Euler angle α^0_{RL} describes the orientation of the rotor with respect to the laboratory frame at time t_0. Recoupling sequences suitable for measuring shift parameters result in a transverse single-quantum Hamiltonian that takes the form

$$H^{(1)} = \sum_j \left(\omega_j T_{1-1} + \omega_j^* T_{11}\right)$$

to first order, where the index j runs over all chemical shift interactions. The coefficients ω_j depend on the spatial part of the chemical shift interaction, as well as the scaling factor. For ^{1}H suitable sequences must avoid inadvertently recoupling the homonuclear dipolar interaction and the isotropic shift, while first-order compensation for rf amplitude inhomogeneity can also be included [24]. Many symmetries fit these criteria, but several additional factors must be considered when selecting a recoupling sequence for use with ultrafast MAS. In particular the pulse sequence is synchronized with the spinning, so that many symmetries requiring a large ratio ω_1/ω_r become impractical at higher MAS rates. For example, $\mathrm{R18}^5_2$ and $\mathrm{R12}^4_1$ require rf amplitudes in excess of 180 kHz and 240 kHz, respectively, for MAS rates above 40 kHz.

Experimental

The pulse sequence used to record ^{1}H anisotropic-isotropic shift correlation spectra has been described previously in Ref. [5] Experiments were recorded at a ^{1}H Larmor frequency of 850.22 MHz, using a double-resonance 1 mm MAS probe. A MAS rate of 78.0 kHz was selected, so that the π pulse duration in the $\mathrm{R16}^2_3$ recoupling sequence was 2.4 μs corresponding to a ^{1}H rf amplitude of 208.3 kHz. There were 64 t_1 increments with data points sampled every 12 R elements, resulting in a dwell time in the indirect dimension of 28.8 μs.

Experiments used a pre-saturation pulse train of 200 $\pi/2$ pulses of duration 1.2 μs with successive pulses separated by a delay of 1 ms. For a more detailed description of the pulse sequence see Ref. [5].

The anisotropy and asymmetry parameters for the chemical shift are defined according to $\zeta = \delta_{zz} - \delta_{iso}$ and $\eta = (\delta_{yy} - \delta_{xx})/\zeta$, respectively, with the principal components ordered according to $|\delta_{zz} - \delta_{iso}| \geq |\delta_{xx} - \delta_{iso}| \geq |\delta_{yy} - \delta_{iso}|$. Numerical simulations of the recoupled ^{1}H CSA lineshapes were performed using SIMPSON [25]. Powder averaging was achieved using 615 (α,β) orientations chosen according to the scheme of Zaremba [26] and 5 uniformly distributed values of γ. B_1 inhomogeneity was included by summing 13 simulations carried out using rf amplitudes weighted according to the experimentally determined B_1 distribution, as determined using the experiment of Odedra and Wimperis [27]. The image of the B_1 distribution for the 1 mm probe obtained with this experiment is shown in the Supporting Information (Figure S1). To extract the ^{1}H CSAs an array of simulated lineshapes was generated for a suitable range of ζ values and η between 0.0 to 1.0, and the ^{1}H shift tensor parameters were extracted by comparing these with the experimental data, using a similar method to that described in Ref. [5]. For each simulated lineshape the optimal scaling was found by fitting to the experimental data, and the corresponding χ^2 parameter was plotted as a function of ζ and η. The resulting error surface allows the best-fit values of ζ and η to be obtained, as well as their confidence limits, assuming χ^2 is normalized [28] according to

$$\chi^2 = \frac{1}{\nu}\sum_{i=1}^{n}\frac{\left(Y_i - E_i\right)^2}{e^2}$$

where E is the experimental spectrum, Y is the simulated spectrum, n is the total number of data points, e is the standard deviation due to noise, and ν is the number of degrees of freedom $n - p - 1$ where p is the number of fit parameters. It should be noted that the effects of B_1 inhomogeneity can be minimized more directly using modified recoupling sequences with composite R elements, [6] allowing more accurate measurements of smaller CSAs by removal of spurious intensity close to $n_1 = 0$. However, for L-ascorbic acid significant ν_2 spectral overlap between sites with large and small CSAs (see below) reduces the benefits of this approach.

Computational

Hydrogen atom positions in crystal structures obtained from the Cambridge Structural Database were optimized with the CASTEP DFT package [29]. Wavefunctions were expanded in terms of plane waves with

ultrasoft pseudo-potentials to represent the core electrons. The PBE approximation [30] to the exchange-correlation interaction was used, and the Brillouin zone was sampled using a Monkhorst-Pack grid of k-points. The optimized energy was converged to within ±0.01 eV, firstly by increasing the cut-off energy for the plane-wave expansion in steps from 100 to 1000 eV and subsequently by decreasing the spacing of the Monkhorst-Pack grid in steps from 0.1 to 0.05 $Å^{-1}$. ^{1}H NMR parameters were calculated for each structure from the database before and after geometry optimization, and this was achieved using the gauge-including projector augmented-wave [20] (GIPAW) approach, as implemented in CASTEP. The principal components of the resulting shielding tensor were obtained by diagonalizing its symmetric part. Chemical shifts are measured relative to a reference frequency with their direction opposite to the shielding, so the isotropic chemical shift was calculated from the isotropic average of the shielding tensor according to

$$\delta_{iso} = -\left(\sigma_{iso} - \sigma_{ref}\right)$$

The principal components of the chemical shift tensor were obtained from those of the shielding tensor in a similar fashion. Following standard practice [31] the ^{1}H reference shielding was obtained for each optimized structure by fitting the calculated isotropic shifts to the experimental values with σ_{ref} as a variable parameter. The reference shieldings obtained for the different crystal structures were 30.51 ± 0.05 ppm in good agreement with values in the literature [31-33]. To compare with experimental data two-dimensional anisotropic-isotropic correlation spectra were simulated using SIMPSON from the calculated principal components of all 16 ^{1}H sites using the measured B_1 distribution and the experimental ν_2 linewidths obtained from the ^{1}H ultrafast MAS spectrum.

Results and Discussion

Ascorbic Acid Crystal Structures

Several crystal structures for L-ascorbic acid have been published previously and have been extracted from the Cambridge Structural Database (CSD). [34] These include X-ray structures obtained at both ambient temperature (lascac10) [35] and at low temperatures: 120 K (lascac12) [36], 100 K (lascac14) and 90 K (lascac15) as well as a neutron diffraction refinement (lascac01) [37] of the hydrogen atom positions in the ambient temperature structure. In all cases the space group is $P2_1$, and there are four L-ascorbic acid molecules in the unit cell and two in the asymmetric unit, related to one another by a pseudo symmetry operation. The five-membered ring of the L-ascorbic acid molecule is almost planar and the side chain has an

extended conformation, as shown in Figure S2. There are eight distinct intermolecular hydrogen bonds, consisting of two helical series of three OH…O bonds and two isolated OH…O bonds. Within the two helices the donor-acceptor sequence is reversed in the two inequivalent molecules. In the neutron structure the H…O bond lengths range from 1.629 to 2.048 Å, while in the 100 K X-ray structure these are slightly longer ranging from 1.645 to 2.103 Å. Although there are some differences in axis system and atom labelling, the conformations of the molecules are very similar in all structures, with the same hydrogen-bond network and no significant differences for bond angles and bond distances between the non-hydrogen atoms. The unit cell volume is 2.2 % smaller in the 120 K structure.

^{1}H Shift Parameters

Figure 1 shows ^{1}H ultrafast MAS spectra of L-ascorbic acid recorded at (a) a magnetic field of 14.095 T and a MAS rate of 62.5 kHz and (b) a magnetic field of 19.969 T and a MAS rate of 78.0 kHz. A modest resolution gain results from the simultaneous increase of both magnetic field and MAS rate with a previously unresolved hydrogen-bonded ^{1}H resonance appearing as a shoulder at 6.1 ppm. Nevertheless, only one of the eight inequivalent hydrogen-bonded sites (at 9.1 ppm) in L-ascorbic acid is fully resolved in the one-dimensional spectrum even at the higher magnetic field and MAS rate. The two-dimensional anisotropic-isotropic correlation spectrum recorded as described in the Experimental Section is shown in Figure 2(a). In contrast to the one-dimensional ^{1}H ultrafast spectrum this allows three hydrogen-bonded ^{1}H sites at δ_2 = 9.1, 7.2 and 6.1 ppm to be clearly identified, since they result in well-resolved recoupled CSA lineshapes in ν_1. Two further hydrogen-bonded ^{1}H sites at δ_2 = 4.9 and 4.0 ppm can be resolved in the correlation spectrum, since their recoupled CSA lineshapes extend well beyond the narrow response from the remaining ^{1}H sites in ν_1. The intense response at δ_2 = 11.1 ppm comprises the remaining three of the expected eight hydrogen-bonded ^{1}H sites which are not resolved. Cross-sections (black lines) parallel to ν_1 taken at the δ_2 shifts corresponding to the three well-resolved hydrogen-bonded ^{1}H sites are shown in Figure 2(b), together with SIMPSON simulations (grey lines) produced according to the method described in the experimental section for the best-fit chemical shift parameters (see Table 1). The corresponding error surfaces are given in the Supplementary Information (Figure S3). The poor fit in the centre of some lineshapes is due to a zero-frequency peak which has been discussed extensively in Refs. [1,5,6].

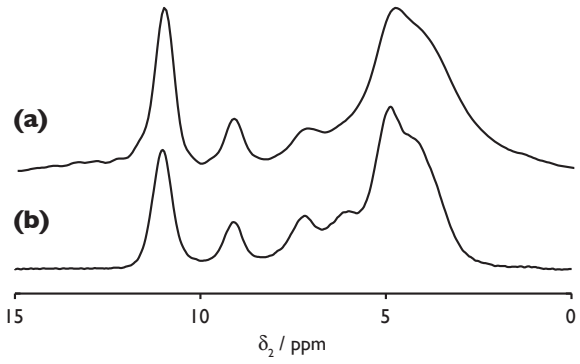

Figure 1. ^{1}H MAS NMR spectra of L-ascorbic acid recorded at (a) a B_0 field strength of 600 MHz and a MAS rate of 62.5 kHz and (b) a B_0 field strength of 850 MHz and a MAS rate of 78 kHz.

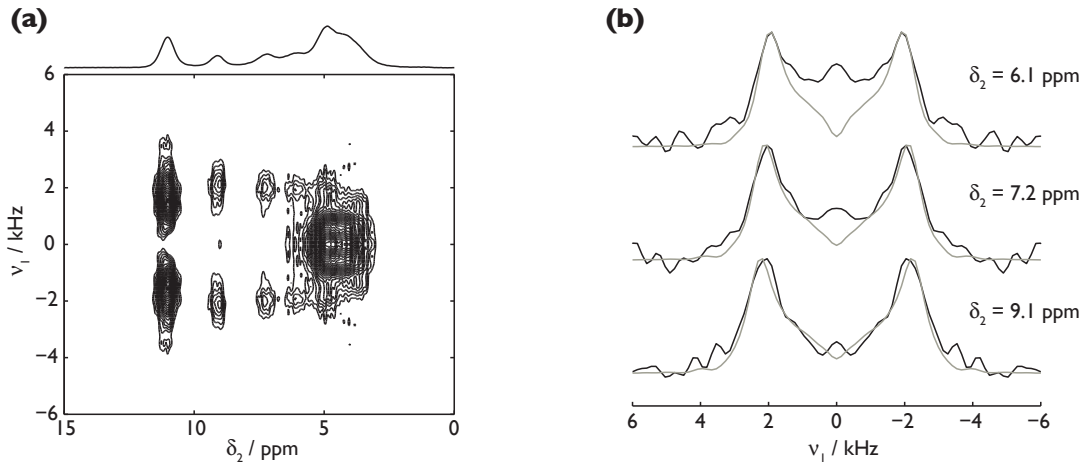

Figure 2(a) Experimental anisotropic-isotropic correlation spectrum for ascorbic acid recorded at a Larmor frequency of 850.22 MHz and a MAS rate of 78.0 kHz. **(b)** Cross-sections (black lines) parallel to ν_1 showing recoupled ^{1}H lineshapes and simulations (grey lines) based on the best-fit chemical shift parameters.

Table 1. Experimental values of ^{1}H chemical shift parameters in L-ascorbic acid (with 95% confidence limits) measured in this work from fitting as described in the text.

Site[1]	δ_{iso}	ζ / ppm[2]	η
H10	9.11	21.4 (20.5-22.5)	0.1 (0.0 – 0.6)
H14	7.21	20.2 (19.0-21.3)	0.1 (0.0 – 0.6)
H16	6.06	18.7 (17.7-20.6)	0.2 (0.0 – 0.6)

1. Hydrogen sites numbered according to Ref. [35]. For assignment see Table 3 below.

2. The sign of ζ cannot be determined by the experiment used here.

Structure Refinement

In this contribution we demonstrate that the hydrogen positions in crystals with complex hydrogen-bonding networks can be refined by combining the ultrafast MAS anisotropic-isotropic shift correlation experiment and DFT calculations. The approach is based on the simulation of a full two-dimensional spectrum, so that the quality of the refinement is assessed against the mismatch between experimental and simulated values of both δ_{iso} and ζ. As a consequence any ^{1}H resonance with either a resolved δ_{iso} or a distinct value of ζ can be assigned to a ^{1}H site in the refined crystal structure. Figure 3(a) shows an anisotropic-isotropic correlation spectrum (grey contours) simulated for the published ambient temperature X-ray structure (lascac10) as described in the Computational Section superimposed on the experimental data from Figure 2(a) (black contours). Note that no optimization of the hydrogen atom positions was carried out before simulating this spectrum and that there is a substantial mismatch between the simulated and experimental spectra, demonstrating that the hydrogen bonds in this structure are inconsistent with the NMR parameters. In particular, for the ambient temperature X-ray structure four of the eight intermolecular H…O hydrogen bonds are greater than 2 Å in length and these result in the four peaks between δ_2 = -4.5 and -9.0 ppm. The normalized χ^2 parameter defined above was used to assess the overall fit to the experimental spectrum and was found to be 19.87 for this simulation. Figure 3(b) shows a similar anisotropic-isotropic correlation spectrum (grey contours) simulated for the published neutron refinement of the X-ray structure (lascac01), superimposed on the same experimental data (black contours). In this case, although the fit is still poor, it is significantly improved over the previous simulation with a normalized χ^2 parameter of 8.52.

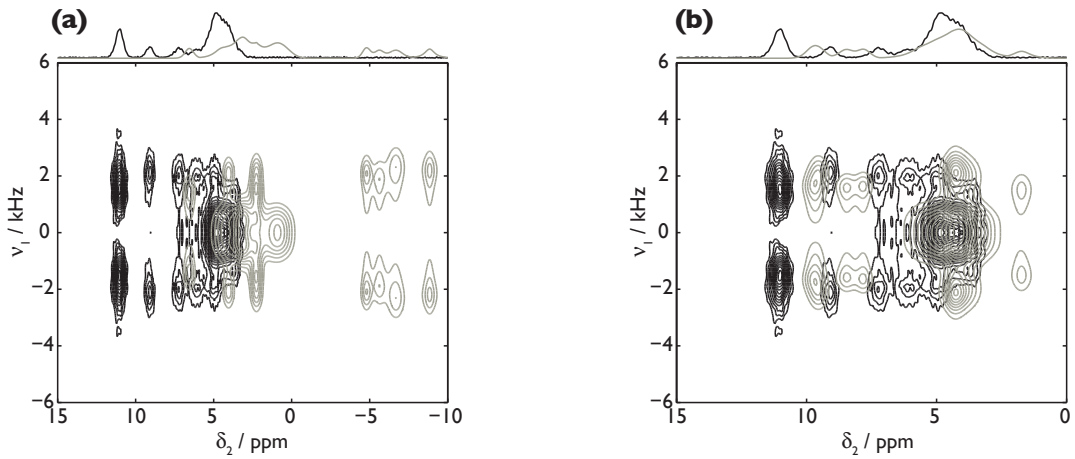

Figure 3(a) Anisotropic-isotropic correlation spectrum (grey contours) simulated for the published ambient temperature X-ray structure (lascac10) superimposed on the experimental data from Figure 2(a) (black

contours). The normalized χ^2 parameter was 19.87. **(b)** As (a) but for the neutron refinement of the X-ray structure (lascac01). The normalized χ^2 parameter was 8.52.

Figure 4(a) shows an overlay of experimental (black contours) and simulated (grey contours) anisotropic-isotropic correlation spectra of L-ascorbic acid. In this case the simulated spectrum was obtained by geometry optimization of the hydrogen positions only, starting from the neutron refinement (lascac01) [37]. The excellent agreement obtained is clearly evident, with the normalized χ^2 parameter reduced to 2.72. As shown in Figure 4(b) excellent agreement was also obtained between pairs of cross-sections through the experimental (black lines) and simulated (grey lines) spectra taken parallel to ν_1 at the isotropic ^{1}H shifts δ_2 indicated. An almost identical simulation was obtained after geometry optimization of the hydrogen positions using the ambient temperature X-ray structure (lascac10) [35] as a starting point, which is expected since the neutron refinement does not alter the heavy atom positions. The normalized χ^2 parameter was monitored as a function of both the cut-off energy for the plane-wave expansion and the spacing of the Monkhorst-Pack grid, and improvements in the overall fit between experiment and simulation closely match decreases in the optimized energy.

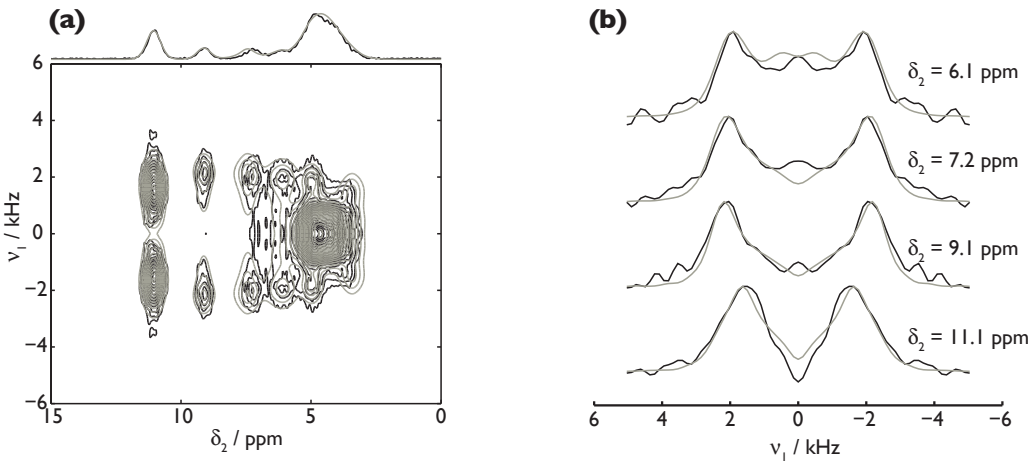

Figure 4(a) Anisotropic-isotropic correlation spectrum (grey contours) simulated for the structure obtained by optimizing the hydrogen positions in the neutron structure (lascac01) superimposed on the experimental data from Figure 2(a) (black contours). The normalized χ^2 parameter was 2.72. **(b)** Cross-sections parallel to ν_1 through the simulated (grey lines) and experimental anisotropic-isotropic correlation spectra from (a) at the isotropic ^{1}H shifts δ_2 indicated.

The results suggest that (as expected) the neutron refinement is more consistent with the NMR data, since the hydrogen atom displacements during geometry optimization are significantly smaller compared with

those for the X-ray structure, as shown in Figure 5. Similar agreement between simulation and experiment was obtained by hydrogen-only geometry optimization starting from the other lower temperature X-ray structures in the CSD. As an example the result for the structure acquired at 120 K (lascac12) due to Milanesio *et al.* [36] is shown in the Supplementary Information (Figure S4). The normalized χ^2 parameter was slightly higher in this case at 4.35, with the difference arising from small variations in heavy atom positions which remain fixed during geometry optimization.

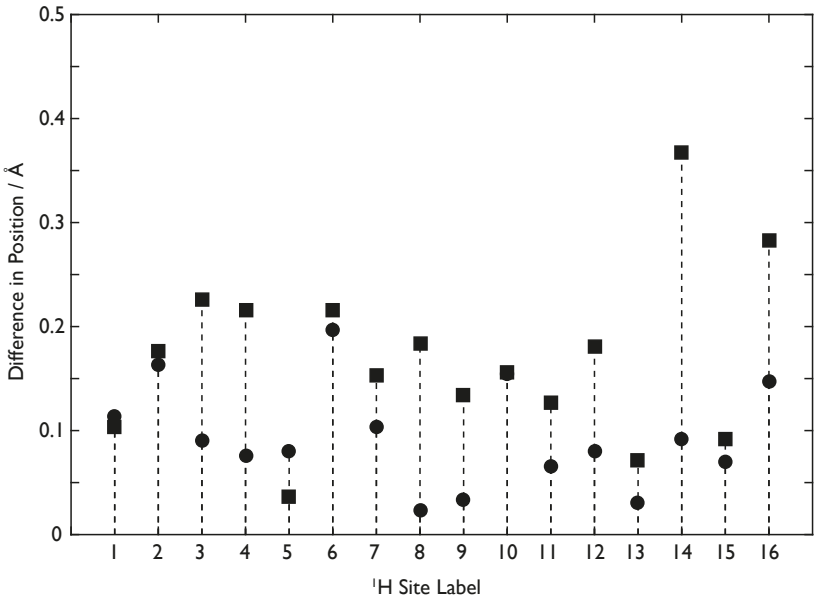

Figure 5. Difference in ^{1}H positions after geometry optimization compared to (circles) neutron refinement (lascac01) and (squares) X-ray structure (lascac10).

Table 2 shows the changes which occur in the hydrogen-bond acceptor (O…H) and donor (H-O) distances during geometry optimization. Note that the initial ambient temperature X-ray structure (lascac10) shows H-O bond lengths which are mostly considerably shorter than the sum of the covalent radii. Neutron refinement (lascac01) and geometry optimization result in successive extensions of the H-O covalent bond, with a concomitant contraction of the O…H hydrogen-bond distance. Apparent changes in the donor-acceptor O…O separation given by the sum of the two distances in the Table result in fact from adjustments to the OH…O angle. It is well known that X-ray and neutron diffraction result in different crystal structures, since X-rays measure maxima in the electron density in the vicinity of the atoms, while neutron diffraction locates the atomic nuclei directly. In bonds with electronegative atoms the hydrogen nucleus and the centre of its electron density do not coincide, so that the positions of hydrogen atoms often differ by more than 0.1 Å in structures determined by the two methods. Nevertheless, neutron diffraction is considered more

reliable, and allows the hydrogen atom positions to be located as accurately as those of heavy nuclei. These results suggest that this NMR crystallography approach can be used to improve X-ray structures without the need for neutron refinement. In addition, the improved resolution in the two-dimensional spectrum allows a complete assignment of the ^{1}H sites to be made, as shown in Table 3.

Table 2. Hydrogen-bond acceptor (A…H) and donor (H-D) distances in Å obtained from geometry optimization (this work), neutron refinement (lascac1) and X-ray diffraction at ambient temperature (lascac10).

Hydrogen-Bond[1]		Geometry Optimized		lascac1		lascac10	
A…H	H-D	A…H	H-D	A…H	H-D	A…H	H-D
O12…H2	H2-O2	1.603	1.023	1.748	0.876	1.748	0.885
O1…H4	H4-O3	1.678	1.011	1.730	0.948	1.869	0.829
O2…H6	H6-O5	1.824	0.989	1.764	1.082	2.001	0.820
O8…H8	H8-O6	2.069	0.966	2.084	0.945	2.230	0.817
O11…H10	H10-O8	1.638	1.011	1.629	1.045	1.773	0.871
O7…H12	H12-O9	1.692	1.010	1.718	0.978	1.833	0.929
O6…H14	H14-O11	1.723	0.999	1.787	0.935	2.044	0.738
O5…H16	H16-O12	1.805	0.994	1.847	0.956	2.024	0.774

1. Sites numbered according to Ref. [35]

Table 3. Assignment of the ^{1}H spectrum and values of calculated ^{1}H chemical shift parameters in L-ascorbic acid obtained as described in the text.

Site[1]	Calculated			Experimental[2]
	δ_{iso}	ζ	η	δ_{iso}
H1	3.82	2.97	0.97	3.8
H2	11.08	-21.01	0.15	11.1
H3	4.75	-4.14	0.78	4.8
H4	11.04	-14.99	0.21	11.1
H5	5.02	-3.62	0.62	4.8
H6	4.95	-17.55	0.21	4.8
H7	4.45	-3.37	0.70	3.8
H8	3.43	-14.50	0.42	3.8
H9	4.13	-3.38	0.64	3.8
H10	9.12	-20.73	0.10	9.1
H11	4.54	-4.29	0.60	4.8
H12*	11.07	-15.47	0.29	11.1
H13	5.12	-3.63	0.80	4.8
H14	7.44	-20.31	0.15	7.2
H15	4.38	-3.34	0.78	3.8
H16	6.05	-18.63	0.20	6.1

1. Hydrogen sites numbered according to Ref. [35]

2. Experimental ^{1}H spectrum deconvoluted into 6 lines.

Experimental measurements of $\delta_{iso}(^1H)$ and CSA(^{1}H) at ambient temperatures are affected by molecular motions which are not included in calculations based on a single static structure, but it has been shown [38] that these can be taken into account by averaging over vibrational configurations. In the light of this, the apparently excellent agreement obtained here between experimental and simulated anisotropic-isotropic correlation spectra requires further investigation, and this is currently underway. Note that the observed improvement results in large part from a correction for the substantial underestimate of the H-D covalent bond length in the X-ray structure (lascac10). The agreement obtained in this case suggest that this contribution is more significant in this case than temperature effects. Furthermore, relatively weak hydrogen bonds as here are associated with asymmetric potential energy curves with the hydrogen atom located in a relatively deep minima close to the donor oxygen, such that the variation with temperature is expected to be less than for stronger hydrogen bonds.

Conclusion

A ^{1}H anisotropic-isotropic shift correlation experiment which employs symmetry-based recoupling sequences to reintroduce the chemical shift anisotropy in ν_1 and ultrafast MAS to resolve ^{1}H sites in ν_2 has been described. This experiment has been used to measure ^{1}H shift parameters for L-ascorbic acid, and the ^{1}H CSAs of hydrogen-bonded sites with resolved isotropic shifts have been extracted directly from the recoupled lineshapes. In combination with DFT calculations, hydrogen positions in crystal structures obtained from X-ray and neutron diffraction have been refined by comparison with simulations of the full two-dimensional spectrum.

Acknowledgements

HM and RC thank the EPSRC and the University of Nottingham for PhD studentships. The UK 850 MHz solid-state NMR Facility used in this research was funded by EPSRC and BBSRC, as well as the University of Warwick, including part funding through Birmingham Science City Advanced Materials Projects 1 and 2, supported by Advantage West Midlands (AWM) and the European Regional Development Fund (ERDF).

References

[1] D. H. Brouwer and J. A. Ripmeester, *J. Magn. Reson.*, 2007, **185**, 173–178.
[2] M. H. Levitt, *J. Chem. Phys.*, 2008, **128**, 052205.
[3] M. Carravetta, M. Eden, X. Zhao, A. Brinkmann and M. H. Levitt, *Chem. Phys. Lett.*, 2000, **321**, 205–215.
[4] G. Hou, S. Paramasivam, S. Yan, T. Polenova and A. J. Vega, *J. Am. Chem. Soc.*, 2013, **135**, 1358–1368.
[5] H. K. Miah, D. A. Bennett, D. Iuga and J. J. Titman, *J. Magn. Reson.*, 2013, **235**, 1–5.
[6] M. K. Pandey, M. Malon, A. Ramamoorthy and Y. Nishiyama, *J. Magn. Reson.*, 2015, **250**, 45–54.
[7] R. Zhang, K. H. Mroue and A. Ramamoorthy, J. Chem. Phys., 2015, **143**, 144201.
[8] B. Berglund and R. W. Vaughan, *J. Chem. Phys.*, 1980, **73**, 2037-2043.
[9] C. M. Rohlfing, L. C. Allen and R. Ditchfield, *J. Chem. Phys.*, 1983, **79**, 4958-4966.
[10] G. A. Jeffrey and Y. Yeon, *Acta Crystallogr. B*, 1986, **42**, 410–413.
[11] J. P. Yesinowski and H. Eckert, *J. Am. Chem. Soc.*, 1987, **109**, 6274–6282.
[12] H. Eckert, J. P. Yesinowski, L. A. Silver and E. M. Stolper, *J. Phys. Chem.*, 1988, **92**, 2055–2064.
[13] H. Rosenberger, G. Scheler and Y. N. Moskvich, *Magn. Reson. Chem.*, 1989, **27**, 50–56.
[14] T. K. Harris, Q. Zhao and A. S. Mildvan, *J. Mol. Struct.*, 2000, **552**, 97–109.
[15] R. K. Harris, P. Jackson, L. H. Merwin, B. J. Say and G. Hagele, *J. Chem. Soc., Faraday Trans. 1*, 1988, **84**, 3649–3672.
[16] E. Brunner and U. Sternberg, *Prog. Nucl. Magn. Reson. Spectrosc.*, 1998, **32**, 21–57.
[17] T. Emmler, S. Gieschler, H. H. Limbach and G. Buntkowsky, *J. Mol. Struct.*, 2004, **700**, 29–38.
[18] G. Wu, C. J. Freure and E. Verdurand, *J. Am. Chem. Soc.*, 1998, **120**, 13187–13193.
[19] A. L. Webber, B. Elena, J. M. Griffin, J. R. Yates, T. N. Pham, F. Mauri, C. J. Pickard, A. M. Gil, R. Stein, A. Lesage, L. Emsley and S. P. Brown, *Phys. Chem. Chem. Phys.*, 2010, **12**, 6970–6983.
[20] C. J. Pickard and F. Mauri, *Phys. Rev. B*, 2001, **63**, 245101.
[21] R. K. Harris, P. Y. Ghi, R. B. Hammond, C.-Y. Ma and K. J. Roberts, *Chem. Commun.*, 2003, 2834-2835.
[22] M. Baias, J.-N. Dumez, P. H. Svensson, S. Schantz, G. M. Day and L. Emsley, *J. Am. Chem. Soc.*, 2013, **135**, 17501–17507.
[23] G. M. Day, *Crystallography Reviews*, 2011, **17**, 3–52.
[24] M. H. Levitt, *Symmetry-Based Pulse Sequences in Magic-Angle Spinning Solid-State NMR*, John Wiley & Sons, Ltd, Chichester, UK, 2007
[25] M. Bak, J. T. Rasmussen and N. C. Nielsen, *J. Magn. Reson.*, 2000, **147**, 296–330.
[26] S. K. Zaremba, *Ann. Mat. Pura. Appl.*, 1966, **73**, 293–317.
[27] S. Odedra and S. Wimperis, *J. Magn. Reson.*, 2013, **231**, 95–99.
[28] W. T. Eadie, D. Drijard, F. E. James, M. Roos and B. Sadoulet, *Statistical Methods in Experimental Physics*, North Holland Publishing Co., Amsterdam, 1971.
[29] S. J. Clark, M. D. Segall, C. J. Pickard, P. J. Hasnip, M. I. J. Probert, K. Refson and M. C. Payne, *Z. Kristallogr.*, 2005, **220**, 1–4.
[30] J. P. Perdew, K. Burke and M. Ernzerhof, *Phys. Rev. Lett.*, 1996, **77**, 3865–3868.
[31] J. R. Yates, S. E. Dobbins, C. J. Pickard, F. Mauri, P. Y. Ghi and R. K. Harris, *Phys. Chem. Chem. Phys.*, 2005, **7**, 1402-1407.
[32] J. Yates, T. Pham, C. Pickard, F. Mauri, A. Amado, A. Gil and S. Brown, *J. Am. Chem. Soc.*, 2005, **127**, 10216–10220.
[33] M. Kibalchenko, D. Lee, L. Shao, M. C. Payne, J. J. Titman and J. R. Yates, *Chem. Phys. Lett.*, 2010, **498**, 270–276.
[34] C. R. Groom, I. J. Bruno, M. P. Lightfoot and S. C. Ward, *Acta Crystallogr. B*, 2016, **72**, 171–179.
[35] J. Hvoslef, *Acta Crystallogr. B*, 1968, **24**, 23–35.
[36] M. Milanesio, R. Bianchi, P. Ugliengo, C. Roetti and D. Viterbo, *J. Mol. Struct.*, 1997, **419**, 139–154.
[37] J. Hvoslef, *Acta Crystallogr. B*, 1968, **24**, 1431–1440.
[38] J.-N. Dumez and C. J. Pickard, *J. Chem. Phys.*, 2009, **130**, 104701.